RSC Advances

PAPER

View Article Online
View Journal | View Issue

Cite this: *RSC Adv.*, 2026, **16**, 11348

Comprehensively investigating pharmacokinetics and metabolic fate of andrographolide in rats by liquid chromatography/mass spectrometry-based approach

Xuelin Sun,[a] Yatong Zhang,[a] Zhanpeng Shang,[b] Lin Dou,[c] Tianying Wang,[d] Jiantao Qiu*[e] and Shuang Chen*[f]

Andrographolide, a natural labdane diterpenoid lactone isolated from *Andrographis paniculata*, possesses diverse pharmacological properties such as anti-tumor, anti-inflammatory, antiviral, and immunomodulatory activities, rendering it a promising candidate for therapeutic development. In this study, pharmacokinetic profiles, excretion features, and metabolism of andrographolide were systematically investigated in rats using a liquid chromatography/mass spectrometry (LC/MS)-based approach. Following intravenous and oral administration, andrographolide exhibited high elimination and moderate bioavailability. Excretion study revealed that less than 5% of the administered dose was eliminated in its parent form in urine and feces. Metabolic profiling identified a total of 39 analytes, among which 34 were sulfated conjugates—establishing sulfation as the most structurally diverse metabolic pathway of andrographolide in rats. A novel MS/MS fragmentation workflow was established, which enabled the unambiguous discrimination of four sulfation modification sites: *O*-sulfation at the C3 and C19 positions, and *C*-sulfation at the C12 and C14 positions. Collectively, this comprehensive study delineates the complete *in vivo* disposition of andrographolide in rats and clarifies the site-specific sulfation rules of its metabolites.

Received 10th November 2025
Accepted 9th February 2026

DOI: 10.1039/d5ra08654j

rsc.li/rsc-advances

1. Introduction

Andrographolide, a natural labdane diterpenoid lactone derived from *Andrographis paniculata* (commonly known as ChuanXinLian), is characterized by an electrophilic α-alkylidene-β-hydroxy-γ-butyrolactone moiety.[1,2] This structural feature possibly enables covalent and irreversible binding to cellular targets and proteins.[3,4] Owing to this unconventional binding mechanism, andrographolide was reported to exhibit a broad spectrum of pharmacological activities, including anti-tumor,[5] anti-inflammatory,[6] anti-pyretic,[7] antibacterial,[8] antiviral,[9] immunomodulatory,[9] and other properties.[10] Despite its promising efficacy, andrographolide suffered from limited oral bioavailability, while andrographolide sulfonates also exhibited potent bioactivities.[11,12] Therefore, a thorough understanding of the pharmacokinetics and metabolism of andrographolide is essential to elucidate its pharmacological mechanisms and therapeutic potential.

Liquid chromatography coupled with mass spectrometry (LC/MS) is a cornerstone technique for the chemical analysis of natural products,[13–15] and also has been extensively employed in drug metabolism and pharmacokinetic research.[16–18] In a previous study, we developed an approach based on diagnostic product ions (DPI) and neutral loss fragments (NLF) that led to the identification of 148 piperine metabolites in rats, more than 90% of which were previously unreported.[19] For andrographolide, an earlier investigation identified 13 metabolites in liver microsomes and highlighted notable interspecies differences in metabolism across humans, dogs, and rats.[16] Additionally, Yang *et al.* used LC/MS to assess the pharmacokinetic behavior of andrographolide in rats, revealing its high elimination rate.[17] Despite these advances, critical aspects of andrographolide's *in vivo* absorption, excretion, and metabolism remain poorly understood.[16,20,21] This incomplete elucidation of its pharmacokinetic profile poses a substantial barrier to

[a]*Department of Pharmacy, Beijing Hospital, National Center of Gerontology, Institute of Geriatric Medicine, Chinese Academy of Medical Sciences, Beijing, 100730, P. R. China*

[b]*School of Pharmaceutical Sciences, Peking University, Beijing, 100083, P. R. China*

[c]*The Key Laboratory of Geriatrics, Beijing Institute of Geriatrics, Institute of Geriatric Medicine, Chinese Academy of Medical Sciences, Beijing Hospital/National Center of Gerontology of National Health Commission, Beijing, 100730, P. R. China*

[d]*Clinical Research Center, Qingdao Hospital, University of Health and Rehabilitation Sciences (Qingdao Municipal Hospital), Qingdao, 266003, P. R. China*

[e]*Department of Cardiovascular Surgery, The Affiliated Hospital of Qingdao University, Qingdao, 266003, P. R. China. E-mail: qiu_jiantao21@163.com*

[f]*Clinical Laboratory, Qingdao Hospital, University of Health and Rehabilitation Sciences (Qingdao Municipal Hospital), Qingdao, 266003, P. R. China. E-mail: csman1986@126.com*

its further development as a therapeutic agent, particularly in regard to efficacy validation and toxicity assessment.

In the present study, we conducted a comprehensive investigation to elucidate the pharmacokinetic behavior, excretion, and metabolism of andrographolide in rats. The pharmacokinetic profile was initially characterized following both intravenous and oral administration. Intravenous (IV) injection revealed the high elimination nature, whereas oral (PO) dosing resulted in limited systemic bioavailability. Furthermore, systematic metabolite profiling demonstrated that andrographolide was predominantly eliminated in metabolized form. Notably, instability in the gastrointestinal tract was a possible factor contributing to its limited oral absorption.

2. Materials and methods

2.1 Chemicals and reagents

Methanol and acetonitrile (LC/MS grade) were obtained from Fisher Scientific (NJ, USA). Formic acid (LC/MS grade) was purchased from Sigma-Aldrich (MO, USA). Deionized water was purified using a Milli-Q water purification system (Millipore, MA, USA). Andrographolide and bergenin (used as an internal standard, IS) were supplied by DeSiTe Phytochemicals Co., Ltd (Sichuan, China), both with a purity greater than 98% as determined by HPLC-UV analysis.

2.2 Animal experiments

Nine male Sprague-Dawley (SD) rats (body weight: 220 ± 20 g) were obtained from SiBeiFu Experimental Animal Co., Ltd (Beijing, China). The animals were housed under controlled environmental conditions, including a temperature of 24 ± 2 °C, relative humidity of 70 ± 5%, and a 12 h/12 h light/dark cycle. After a 3 days acclimatization period, the rats were randomly assigned to three groups (n = 6 per group): intravenous administration (IV, 2 mg kg^{-1}), oral administration (PO, 20 mg kg^{-1}), and control. All animals were fasted for 12 h with free access to water prior to the experiment. The experimental procedures were approved by the Animal Care and Use Committee of Peking University and conducted in accordance with the Guide for the Care and Use of Laboratory Animals (National Research Council, 1996, USA).

2.3 Preparation of standard solution and quality control solution

Appropriate amounts of andrographolide and the internal standard (IS) were accurately weighed and separately dissolved in methanol to prepare stock solutions at a concentration of 1 mg mL^{-1}, which were stored at 4 °C. The IS stock solution was further diluted with methanol to obtain a working solution at a concentration of 1 μg mL^{-1}. A series of working standard solutions of andrographolide were prepared by serial dilution of the stock solution with methanol. Calibration standards were constructed by spiking appropriate volumes of the working solutions into blank biological matrix to achieve effective andrographolide concentrations of 2, 5, 20, 50, 200, 500, and 1000 ng mL^{-1}. Quality control (QC) samples were prepared similarly at low, medium, and high concentrations (5, 50, and 800 ng mL^{-1}).

2.4 Drug administration and biological samples preparation

2.4.1 Drug administration and sample collection. For IV group, andrographolide was dissolved in a vehicle consisting of 10% DMSO and 90% hydroxypropyl-β-cyclodextrin at a concentration of 2 mg mL^{-1}. For PO group, andrographolide was suspended in 0.5% methylcellulose solution at 2 mg mL^{-1}. The IV group received a dose of 2 mg kg^{-1} body weight, while the PO group received 20 mg kg^{-1}. Blood samples (0.5 mL) were collected from the suborbital venous plexus at 0.25, 0.5, 1, 2, 4, 8, and 24 h after drug administration. The samples were centrifuged at 3500 rpm for 10 min to isolate plasma. Urine was collected over the intervals of 0–4 h, 4–8 h, and 8–24 h following oral administration. Feces were collected at 0–4 h, 4–8 h, 8–24 h, 24–32 h, and 32–48 h, and homogenized with a fourfold volume of saline.

2.4.2 Sample preparation. Sample preparation for pharmacokinetic and excretion studies was performed as follows: 20 μL of plasma, 50 μL of urine, or 50 μL of fecal homogenate was aliquoted into 1.5 mL polypropylene tubes. Subsequently, 300 μL of IS working solution was added to each tube, and the mixtures were vortex-mixed for 2 min and centrifuged at 13 500 rpm for 15 min. Approximately 250 μL of the supernatant was carefully transferred to a fresh tube and evaporated to dryness under a gentle stream of nitrogen. The residue was reconstituted in 100 μL of 5% acetonitrile in water (v/v), vortex-mixed for 2 min to achieve complete solubilization, and centrifuged again at 13 500 rpm for 15 min to remove any insoluble precipitates. The supernatant was injected into the LC/MS system for quantitative analysis of andrographolide.

For metabolism profiling, biological samples from the same experimental group were pooled using the area-under-the-curve (AUC) method to generate representative samples. Solid-phase extraction (SPE) was subsequently utilized for protein precipitation and sample purification. Prior to sample loading, each SPE cartridge was preconditioned with 2 mL of methanol, followed by 2 mL of deionized water to activate the sorbent. Plasma or urine samples were then loaded onto the preconditioned cartridges, which were subsequently rinsed with 3 mL of deionized water and 3 mL of methanol. The final methanol eluate was collected and evaporated to dryness under a gentle stream of nitrogen at room temperature. The residue was reconstituted in 100 μL of 5% acetonitrile in water (v/v), vortex-mixed thoroughly, and centrifuged at 13 500 rpm for 15 min to pellet any insoluble particulates. The resulting supernatant was injected to LC/MS analysis.

2.5 Instrument and conditions

2.5.1 Pharmacokinetics and excretion study. Liquid chromatographic separation was performed on an Exion LC system (Applied Biosystems/Sciex, USA) equipped with a binary pump, a vacuum degasser, a multi-plate autosampler, and a thermostated column compartment. Separation was achieved using a Waters XSelect HSS T3 column (2.1 × 50 mm, 2.5 μm; Waters,

Milford, MA, USA) maintained at 50 °C. The mobile phase consisted of 0.1% formic acid in water (solvent A) and acetonitrile (solvent B), delivered at a flow rate of 600 μL min^{-1} under the following gradient program: 0–0.2 min, 10% B; 0.2–1.0 min, 10–95% B; 1.0–1.5 min, 95% B; 1.5–1.6 min, 95–10% B; 1.6–2.0 min, 10% B. The injection volume was 10 μL. The autosampler was set at 4 °C.

Mass spectrometric detection was performed using an AB SCIEX Triple Quad 5500 plus mass spectrometer utilized in negative ionization mode. Optimized ion source parameters were configured as follows: ion spray voltage, −4000 V; turbo heater temperature, 450 °C; nebulizing gas (Gas 1), 50 psi; heating gas (Gas 2), 50 psi; curtain gas, 30 psi; and collision gas, 12 psi. Quantification was performed *via* multiple reaction monitoring (MRM) of the following transitions: *m*/*z* 395.0 → 331.1 for andrographolide and *m*/*z* 327.0 → 192.0 for IS. A dwell time of 50 ms was assigned to each transition to ensure sufficient signal-to-noise ratio for accurate quantification. Data acquisition and processing were conducted using Analyst Software (version 1.7.2).

2.5.2 Metabolism study. Liquid chromatography analysis was performed using a Ultimate 3000 UHPLC system (Thermo Fisher Scientific, MA, USA) equipped with a binary pump, an autosampler, and a thermostated column compartment. Chromatographic separation was carried out on a Waters ACQUITY BEH C18 column (2.1 × 100 mm, 1.7 μm; Waters Corporation, Milford, MA, USA) maintained at 40 °C. The mobile phase consisted of 0.1% formic acid in water (solvent A) and acetonitrile (solvent B), delivered at a flow rate of 0.20 mL min^{-1} under the following gradient program: 0–2 min, 5% B; 2–15 min, 5–30% B; 15–17 min, 30–95% B; 17–19 min, 95% B. The injection volume was 10 μL.

Mass spectrometric data were acquired using a Q-Exactive hybrid quadrupole-Orbitrap mass spectrometer (Thermo Fisher Scientific, San Jose, CA, USA) equipped with a heated electrospray ionization source operated in negative ion mode. A data-dependent MS^2 acquisition method was employed with the top five most intense precursor ions selected from each full MS scan for fragmentation. Full MS scans were recorded at a resolution of 70 000 FWHM, and MS^2 spectra at 17 500 FWHM. High-purity nitrogen was used as sheath gas (30 arbitrary units), auxiliary gas (10 arbitrary units), and collision gas. A normalized collision energy of 30% was applied. Dynamic exclusion was enabled to avoid repeated fragmentation of abundant ions. Additional source parameters were configured as follows: mass scan range, *m*/*z* 50–800; spray voltage, 3.5 kV; capillary temperature, 350 °C; heater temperature, 350 °C; and S-lens RF level, 55 V.

2.6 Method validation

Selectivity was evaluated by comparing the MRM chromatograms of the blank biological matrix, the matrix spiked with IS only, and the matrix spiked with both IS and andrographolide. Linearity was assessed by constructing calibration curves in rat matrix using the peak area ratio of andrographolide to IS (y) *versus* the nominal concentration (x). A weighted ($1/x^2$) least-squares linear regression model was applied. The lower limit of quantification (LLOQ) was defined as the lowest concentration on the calibration curve that could be quantified with acceptable accuracy and precision, *i.e.*, within ±20% deviation.

To assess the precision and accuracy of the developed method, QC samples at three concentration levels (5, 50, and 800 ng mL^{-1}) were analyzed in five replicates for intra-day and inter-day evaluations. Accuracy was expressed as the relative error (RE, %), while precision was reported as the relative standard deviation (RSD, %). Extraction recovery of andrographolide was determined at each QC level by comparing the peak area ratios (analyte to IS) of pre-extraction samples with those post-extraction spiked samples. Matrix effects were assessed by comparing the peak responses of post-extraction spiked samples (A) with those of neat standard solutions at equivalent concentrations (B), with results expressed as ($A/B \times 100\%$). Storage stability in rat plasma was evaluated under three critical conditions: room temperature (24 °C) for 4 h, autosampler condition (4 °C) for 24 h, and long-term storage for 14 days (−80 °C).

2.7 Pharmacokinetic analysis

Pharmacokinetic parameters were derived using Phoenix WinNonlin software (version 6.2; Pharsight Corporation, USA) *via* a noncompartmental model. For the IV administration group, the following parameters were estimated: initial plasma concentration (C_0), area under the concentration–time curve from zero to the last measurable time point (AUC_{0-t}), area under the curve from zero to infinity ($AUC_{0-\infty}$), elimination half-life ($T_{1/2}$), apparent volume of distribution (V_d), mean residence time (MRT), and total body clearance (CL). For the PO administration group, the parameters included maximum plasma concentration (C_{max}), time to reach C_{max} (T_{max}), AUC_{0-t}, $AUC_{0-\infty}$, $T_{1/2}$, and absolute bioavailability (F).

3. Results and discussion

3.1 Method validation

Representative MRM chromatograms of a blank plasma sample, a blank sample spiked with the andrographolide only, and a blank sample spiked with both IS and andrographolide were presented in Fig. 1. The chromatograms demonstrate a stable baseline and good resolution between andrographolide and the IS, with no observable interference from endogenous substances in their respective detection channels.

Calibration curves for andrographolide in plasma, urine, and feces exhibited good linearity over the concentration range of 2 to 1000 ng mL^{-1}. Each curve was constructed using a weighted least-squares linear regression model with a $1/x^2$ weighting factor. The regression equations were as follows: $y = 0.00138x + 0.00374$ ($r = 0.9938$) for plasma, $y = 0.0354x - 0.0231$ ($r = 0.9947$) for urine, and $y = 0.0414x + 0.0367$ ($r = 0.9973$) for feces. The lower limit of quantification (LLOQ) exhibited accuracy within ±20% relative error (RE), while all other calibration standards (5–1000 ng mL^{-1}) demonstrated accuracy within ±15% RE.

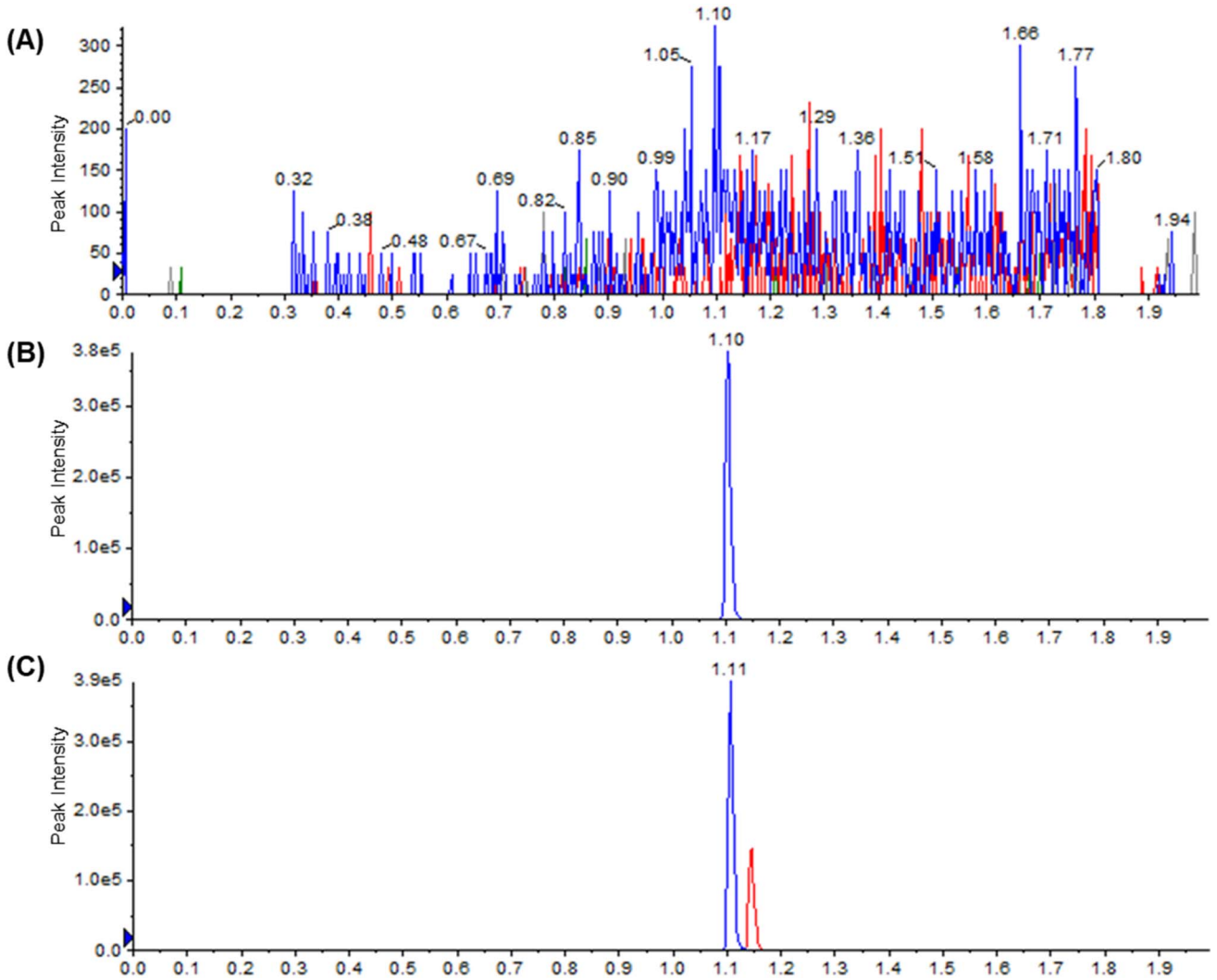

Fig. 1 Typical chromatograms of a blank biological sample (A), a blank biological sample spiked with andrographolide (B), and a blank biological sample spiked with andrographolide and IS (C).

As summarized in Tables S1 and S2, the developed LC-MS/MS method was comprehensively validated for intra-day/inter-day precision, accuracy, matrix effects, and extraction recovery. The intra-day precision (expressed as relative standard deviation, RSD) was 9.32%, 5.28%, and 4.81% for low-, medium-, and high-concentration quality control (QC) samples, respectively. For inter-day precision, the RSD values were 10.24%, 9.27%, and 7.43% for the corresponding QC levels. The mean accuracy for the three QC concentrations was 96.60%, 106.64%, and 95.04%, respectively, reflecting reliable quantitation performance. The mean recovery from spiked plasma samples ranged from 87.54% to 98.45% across different concentration levels, demonstrating consistent and efficient sample extraction. Matrix effects at the three QC levels ranged from 85.74% to 90.51%, with no significant ion suppression or enhancement observed. The storage stability of andrographolide in rat plasma was further verified, and the analyte was confirmed to be stable for at least 4 h at room temperature (24 °C), 24 h in the autosampler (4 °C), and 14 days under long-term storage conditions at −80 °C.

Collectively, these validation data confirm that the established LC-MS/MS method is robust, accurate, and precise, and thus suitable for the quantitative determination of andrographolide in rat plasma for pharmacokinetic analysis.

3.2 Pharmacokinetics and excretion studies

The developed LC/MS method was applied to investigate the pharmacokinetics and excretion of andrographolide following drug administration. Pharmacokinetic parameters derived from noncompartmental analysis were summarized in Table 1, and the mean plasma concentration–time profiles ($n = 6$) were illustrated in Fig. 2A.

After IV administration, the plasma concentration of andrographolide underwent a rapid decline, falling below the LLOQ within 2 hours. Key PK parameters included: $T_{1/2} = 0.18 \pm 0.028$ h, MRT $= 0.16 \pm 0.024$ h, $AUC_{0-t} = 133 \pm 15.5$ h ng mL^{-1}, $V_d = 2.40 \pm 0.25$ L kg^{-1}, $C_0 = 845 \pm 55.9$ ng mL^{-1}, and $CL_{total} = 249 \pm 28.4$ mL min^{-1} kg^{-1}. These data confirm a short *in vivo* residence time and rapid systemic elimination of

Table 1 Pharmacokinetics parameters of andrographolide in rats

Parameters	IV	PO
Dosage (mg kg^{-1})	2	20
T_{max} (hr)	—	1.67 ± 2.02
C_0 (ng mL^{-1})	845 ± 55.9	—
C_{max} (ng mL^{-1})	—	98.9 ± 23.2
AUC_{0-t} (hr × ng mL^{-1})	133 ± 15.5	480 ± 47.7
AUC_{inf} (hr × ng mL^{-1})	135 ± 16.2	618 ± 6.74
V_d (L kg^{-1})	2.40 ± 0.25	—
$T_{1/2}$ (hr)	0.18 ± 0.028	3.22 ± 0.71
MRT (hr)	0.16 ± 0.024	—
CL (mL min^{-1} kg^{-1})	249 ± 28.4	—
F (%)	—	36.1 ± 3.59

andrographolide, consistent with previous reports.[17] Mechanistically, andrographolide is a known substrate of P-glycoprotein (P-gp),[22] an efflux transporter highly expressed in hepatocytes.[23] P-gp mediates the active efflux of andrographolide into bile or the intestinal lumen, increasing apparent clearance independent of metabolic degradation—an effect that contributes to the observed high CL_{total}. Additionally, the short $T_{1/2}$ aligned with the pharmacokinetic equation $T_{1/2} = (0.693 \times V_d)/CL_{total}$, reflecting the combined effects of a small V_d (limited peripheral tissue distribution) and rapid elimination.

Following PO administration, plasma concentrations of andrographolide remained low, with the following PK parameters: $C_{max} = 98.9 \pm 23.2$ ng mL^{-1}, $T_{1/2} = 3.22 \pm 0.71$ h, $AUC_{0-t} = 480 \pm 47.7$ h ng mL^{-1}, and $F = 36.1 \pm 3.59\%$. Notably, the time to reach C_{max} (T_{max}) exhibited substantial variability (1.67 ± 2.02 h), possibly attributed to inter-individual differences in gastrointestinal transit time, intestinal P-gp expression levels, and gut microbiota composition—all of which regulate pre-absorptive sulfation and absorption kinetics of andrographolide.

The cumulative excretion recovery of andrographolide in rat urine and feces following IV administration was illustrated in Fig. 2B. In urine, excretion was predominantly observed within the first 5 hours post-dosing, with 0.075% of the administered parent drug recovered over 24 hours. For feces, the most substantial excretion of parent drug occurred within the first 24 hours, with a total recovery of 1.51% over 48 hours. The pharmacokinetic and excretion data demonstrated that andrographolide was probably exhibited extend metabolism *in vivo*. Consequently, a detailed investigation of andrographolide's metabolic fate was critical for a comprehensive understanding of its *in vivo* disposition and clearance mechanisms.

3.3 Workflow to characterize andrographolide metabolites

3.3.1 Sample pretreatment and MS data-acquisition. Pooled samples were prepared using the AUC pooling method,[25,26] where sample volumes from individual time points were combined proportionally according to time-interval ratio formula: v_1: v_2: …: $v_n = (t_1 - t_0)$: $(t_2 - t_0)$: $(t_3 - t_1)$: …: $(t_n - t_{n-1})$. A data-dependent acquisition strategy combined with dynamic exclusion (apex trigger: 3 s; exclusion duration: 10 s) was employed to maximize coverage of fragment spectra. Parallel reaction monitoring was additionally used as a complementary approach to capture MS/MS data of low-abundance ions. Collectively, these settings ensured the acquisition of comprehensive and high-quality MS/MS data for subsequent structural interpretation.

3.3.2 MS/MS fragmentation behaviors of andrographolide. The MS/MS fragmentation pattern of andrographolide was systematically characterized to enable structural identification of its metabolites (Fig. 3). Andrographolide exhibited an enhanced ion response in negative mode, a property attributable to its intrinsic hydroxyl moieties that facilitate facile deprotonation of the parent molecule. In the full-scan MS spectrum, the predominant ions observed were the $[M + HCOOH–H]^-$ adduct at m/z 395.2068 ($C_{21}H_{31}O_7$, error 0.91 ppm) and the deprotonated molecule $[M–H]^-$ at m/z 349.2015 ($C_{20}H_{29}O_5$, error 1.60 ppm). MS/MS analysis of m/z 349.2015 revealed major fragment ions corresponding to the loss of H_2O yielding $[M–H–H_2O]^-$ at m/z 331.1907 ($C_{20}H_{27}O_4$, error 1.04 ppm), followed by the elimination of CO_2, giving rise to $[M–H–H_2O–CO_2]^-$ at m/z 287.2008 ($C_{19}H_{27}O_2$, error 0.78 ppm).

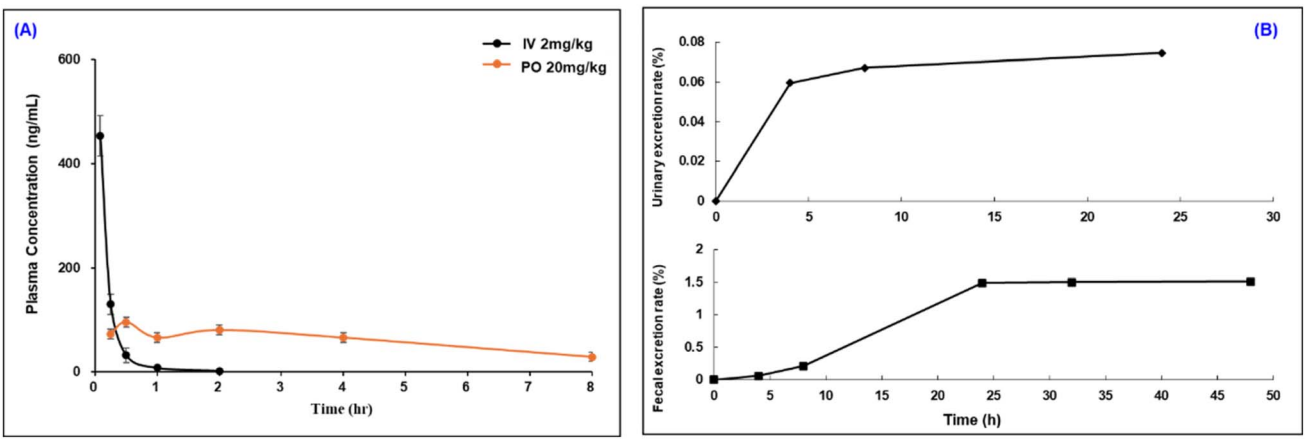

Fig. 2 The mean plasma concentration–time curves of andrographolide after drug administration (A), and cumulative excretions (B) of andrographolide in urine and feces after IV administration.

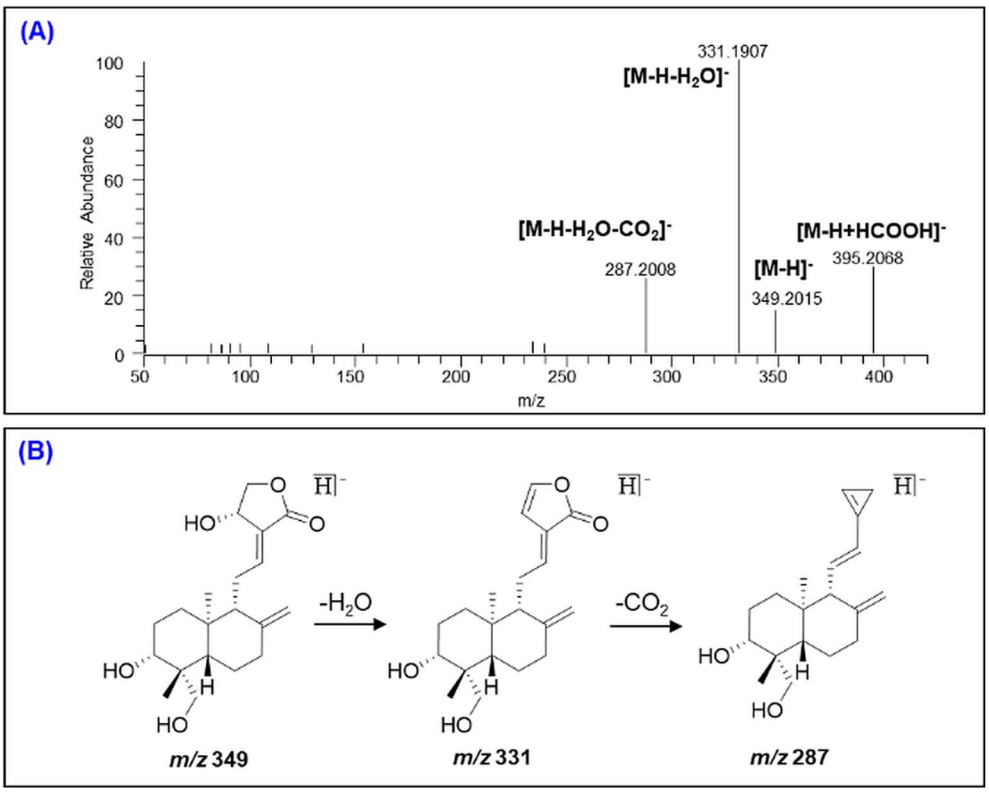

Fig. 3 The MS/MS spectra (A) and proposed mass fragmentation behaviors (B) of andrographolide in the negative ion mode.

3.3.3 MS/MS fragmentation behaviors of sulfated metabolites. Sulfation has been established as a major metabolic pathway for andrographolide *in vivo*.[20,21,24] In MS/MS analysis, sulfated metabolites are inherently prone to fragmentation within electrospray ionization source and yielded characteristic fragment ions. In the present study, the MS/MS fragmentation patterns of known sulfated metabolites were systematically examined (Fig. 4). Based on the sulfation sites, these conjugates were classified into four categories: C3-, C12-, C14-, and C19-sulfated derivatives. Among these derivatives, sulfation at the C12 and C14 positions was designated as *C*-sulfation, whereas sulfation at the C3 and C19 positions was classified as *O*-sulfation.

M13, a well-characterized and validated C12-sulfated metabolite, served as a representative for *C*-sulfated metabolites.[21] In negative ion mode, its MS/MS spectrum displayed a fragment ion at *m*/*z* 79.96, accompanied by a neutral loss of 82 Da (Fig. 4A). This spectral feature indicated a homolytic C–S bond cleavage mechanism. In contrast, sulfation at the C14 position, as observed in metabolite M28, resulted not only in the characteristic neutral loss of 82 Da but also a prominent fragment ion at *m*/*z* 80.96 (Fig. 4D).[21] This pattern indicated a shift toward heterolytic cleavage of the C–S bond, likely

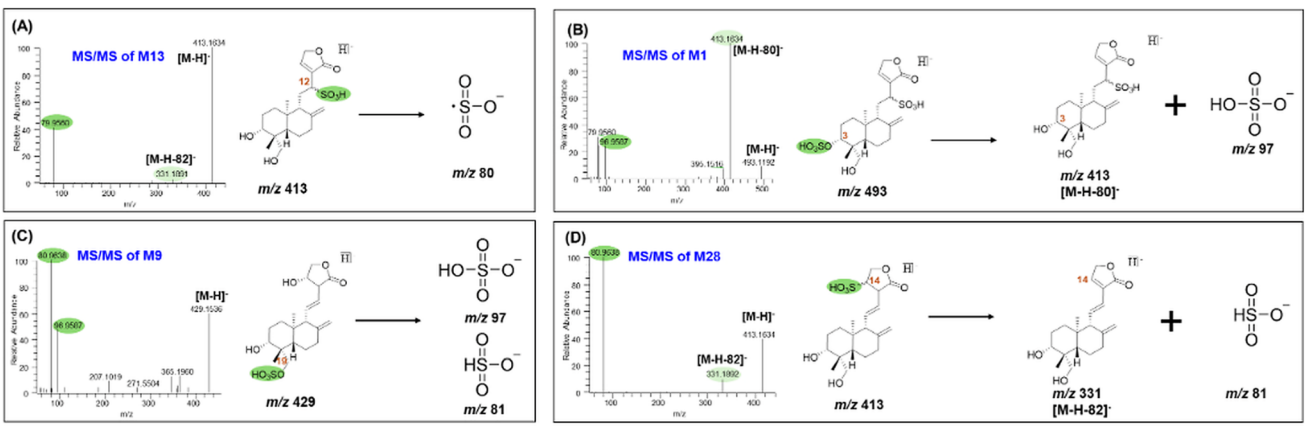

Fig. 4 The MS/MS spectra and pathway of representative sulfation metabolites. *C*-sulfated species at C-12 and C-14 are shown in (A) and (C), respectively, whereas *O*-sulfated species at C-3 and C-19 are shown in (B) and (D), respectively.

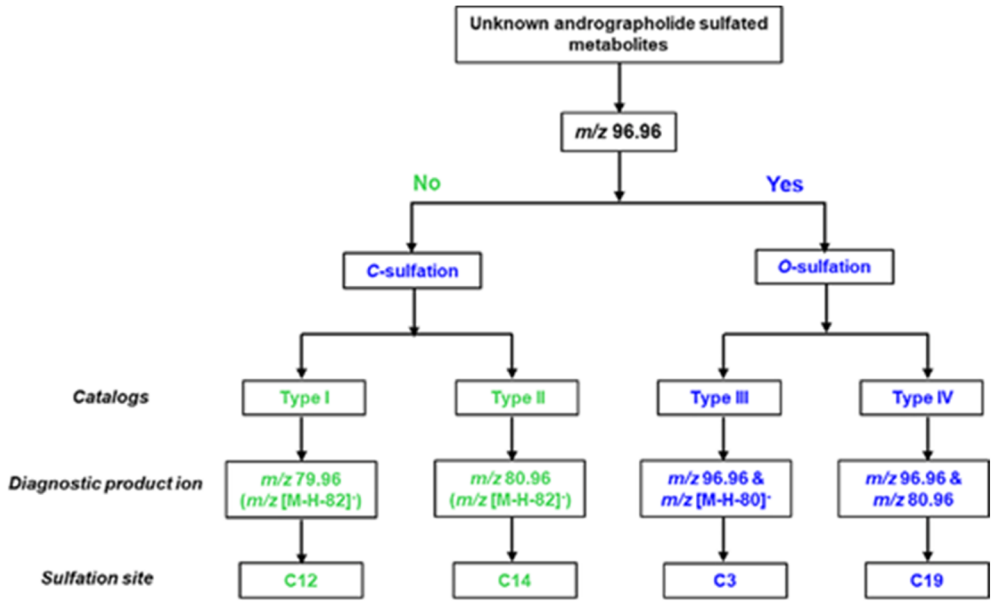

Fig. 5 The flow chart to differentiate unknown sulfation sites of andrographolide metabolites.

influenced by the presence of electron-donating substituents near the sulfation site.

M1 represented a characteristic *O*-sulfated conjugate sulfated at C3, with an additional sulfate group at C12 (Fig. 4B).[21] In addition to the fragment ion at *m*/*z* 79.96 derived from C12-sulfate cleavage, the sulfate moiety at C3 underwent a neutral loss of 80 Da, yielding a prominent $[M–H–80]^-$ product ion. Furthermore, a distinct *m*/*z* 96.96 fragment ion was detected, corresponding to the bisulfate anion ($[HSO_4]^-$). It was proposed to form *via* C–O bond cleavage at the sulfation site, coupled with proton transfer from the β-carbon of the parent scaffold. In contrast, M9 was a prototypical C19 *O*-sulfated conjugate, representative of aliphatic alcohol sulfate derivatives, in which the sulfate moiety was linked to an sp^3-hybridized carbon atom (Fig. 4C).[27,28] Its MS/MS spectrum featured an *m*/*z* 96.96 fragment ion, consistent with $[HSO_4]^-$ formation *via* C–O bond cleavage of the C19 sulfate moiety. An *m*/*z* 80.96 product ion was also detected in the spectrum, which feature corroborated previous findings, and was further validated using a synthetic analog of the metabolite (Fig. S1).

3.3.4 Prediction rules for differentiating sulfation sites of andrographolide metabolites. For each subclass of andrographolide sulfated conjugates, a predominant fragmentation pathway was observed in negative ion mode, which generated distinct structural signatures comprising diagnostic product ions (DPIs) and characteristic neutral loss fragments (NLFs).[30] Our findings demonstrated that the fragmentation profiles of these conjugates were highly dependent on the local structural microenvironment of the sulfation sites on the andrographolide scaffold. Accordingly, the specific sulfation position could be unambiguously deduced by integrating these characteristic fragmentation patterns and diagnostic signature ions. To establish a definitive structure–fragmentation relationship for andrographolide sulfated conjugates, we herein proposed a set of predictive fragmentation rules (Fig. 5).

(1) If a DPI is observed at *m*/*z* 96.97 is detected, the metabolite is identified as an *O*-sulfate conjugate.

(1.1) If a NLF of 80 Da is observed in the absence of other sulfate-associated fragment ions, the sulfate moiety is predominantly localized at the C3 hydroxyl group (C3–OH).

(1.2) If an additional fragment ion at *m*/*z* 80.96 is detected, sulfation likely occurs at an aliphatic alcohol site (*e.g.*, the C19 hydroxyl group, a site bearing a β-hydrogen on an sp^3-hybridized carbon atom.

(2) If a DPI at *m*/*z* 96.97 is absent or present at low relative abundance (<5% relative intensity), the metabolite is categorized as a *C*-sulfated conjugate.

(2.1) If *m*/*z* 79.96 represents the predominant sulfate-associated fragment ion, occasionally accompanied by a NLF of 82 Da, sulfation is assigned to the C12 position.

(2.2) If *m*/*z* 80.96 is the major sulfate-associated fragment ion, along with an occasional NLF of 82 Da, the sulfate moiety is assigned to the C14 position.

3.4 Identification of andrographolide metabolites

A total of 39 metabolites, including the parent drug, were identified in rats following the administration of andrographolide. Of these analytes, 5 were detected in urine, 39 in fecal matrices, and 11 in plasma (Fig. 6), which depicted the distribution profile of all identified analytes across the biological matrices. Detailed analytical and structural characteristics—including retention time, mass spectral data, and metabolic modification types—for each identified analyte were summarized in Table 2.

3.4.1 Characterization of *C*-sulfated conjugates. Four metabolites, namely M13 (retention time 7.57 min), M26 (9.56 min), M28 (10.25 min), and M32 (11.12 min), shared the identical deprotonated molecular ions at *m*/*z* 413.17 ($C_{20}H_{29}O_7S$, error < 1 ppm). In their MS/MS spectra, M13 and M26 displayed

Table 2 Identification of andrographolide metabolites in rats using UHPLC/Orbitrap MS

Peak	t_R (min)	Experimental m/z	Error (ppm)	Formula $[M-H]^-$	MS/MS fragments	Sulfation type	Sulfation site	Other biotransformation	U	P	F
M1	4.09	493.1203	0.36	$C_{20}H_{29}O_{10}S_2$	413.1633, 395.1516, 365.1407, 96.9586, 79.9559	*C*-sulfation & *O*-sulfation	C3 & C12	14-Deoxylation			+
M2[d]	4.42	449.1845	0.09	$C_{20}H_{33}O_9S$	367.2089, 307.1918, 80.9637	*C*-sulfation	C14	Oxidation, di-reduction		+	+
M3[d]	6.16	563.2169	1.24	$C_{25}H_{39}O_{12}S$	545.2050, 331.1908, 80.9638	*C*-sulfation	C14	Reduction, pentosylation			+
M4[d]	6.72	431.1737	−0.52	$C_{20}H_{31}O_8S$	413.1634, 349.2010, 331.1909, 287.2011, 80.9637	*C*-sulfation	C14	Reduction		+	+
M5	6.76	493.1206	0.81	$C_{20}H_{29}O_{10}S_2$	413.1634, 96.9586, 80.9637	*C*-sulfation & *O*-sulfation	C3 & C14	14-Deoxylation			+
M6[d]	6.77	411.1478	0.27	$C_{20}H_{27}O_7S$	331.1907, 96.9586	*O*-sulfation	C3	Dehydration			+
M7[d]	6.93	545.2063	1.18	$C_{25}H_{37}O_{11}S$	463.2348, 331.1905, 79.9559	*C*-sulfation	C12	Pentosylation, dehydration			+
M8[d]	7.03	431.1738	0.53	$C_{20}H_{31}O_8S$	413.1631, 349.2019, 331.1904, 287.2014, 80.9637	*C*-sulfation	C14	Reduction			+
M9[a,c]	7.16	429.1586	0.67	$C_{20}H_{29}O_8S$	365.1965, 347.1846, 96.9587, 80.9637	*O*-sulfation	C19	N.A.			+
M10[d]	7.21	563.2168	1.03	$C_{25}H_{39}O_{12}S$	545.2075, 463.2333, 331.1908, 287.2012, 80.9637	*C*-sulfation	C14	Reduction, pentosylation			+
M11[d]	7.39	411.1479	0.49	$C_{20}H_{27}O_7S$	367.1546, 96.9586, 79.9559	*O*-sulfation	C19	Dehydration			+
M12	7.40	493.1205	0.66	$C_{20}H_{29}O_{10}S_2$	413.1633, 395.1518, 96.9585, 80.9637	*C*-sulfation & *O*-sulfation	C3 & C14	14-Deoxylation			+
M13[b]	7.57	413.1633	−0.02	$C_{20}H_{29}O_7S$	331.1912, 287.2015, 79.9559	*C*-sulfation	C12	14-Deoxylation	+	+	+
M14[d]	7.59	411.1483	1.46	$C_{20}H_{27}O_7S$	381.1369, 299.1647, 255.1748, 79.9559	*C*-sulfation	C12	Dehydration			+
M15[d]	7.80	563.2167	0.92	$C_{25}H_{39}O_{12}S$	545.2052, 331.1917, 287.2007, 80.9637	*C*-sulfation	C14	Reduction, pentosylation			+
M16[d]	7.94	449.1854	1.99	$C_{20}H_{33}O_9S$	369.2298, 309.2062, 96.9587	*O*-sulfation	C3	Oxidation, di-reduction			+
M17[d]	8.01	431.1741	0.46	$C_{20}H_{31}O_8S$	413.1634, 349.2010, 331.1909, 80.9637	*C*-sulfation	C14	Reduction		+	+
M18[d]	8.08	545.2062	1.07	$C_{25}H_{37}O_{11}S$	463.2348, 331.1908, 287.2013, 79.9559	*C*-sulfation	C12	Pentosylation, dehydration			+
M19[d]	8.23	427.1431	1.09	$C_{20}H_{27}O_8S$	365.1418, 345.1698, 79.9559	*C*-sulfation	C12	Dehydrogenation			+
M20[d]	8.34	431.1741	0.525	$C_{20}H_{31}O_8S$	413.1631, 349.2010, 331.1910, 287.2014, 80.9637	*C*-sulfation	C14	Reduction		+	+
M21	8.52	493.1209	1.54	$C_{20}H_{29}O_{10}S_2$	413.1634, 395.1557, 96.9587, 80.9637	*C*-sulfation & *O*-sulfation	C3 & C14	14-Deoxylation			+
M22[d]	8.52	411.1480	0.64	$C_{20}H_{27}O_7S$	96.9586	*O*-sulfation	C19	Dehydration			+
M23[d]	9.00	411.1481	0.93	$C_{20}H_{27}O_7S$	381.1370, 285.1857, 79.9559	*C*-sulfation	C12	Dehydration			+
M24[d]	9.12	449.1841	−0.86	$C_{20}H_{33}O_9S$	369.2275, 96.9585, 80.9637	*O*-sulfation	C19	Oxidation, di-reduction			+
M25[d]	9.13	545.2065	1.62	$C_{25}H_{37}O_{11}S$	463.2348, 331.1913, 79.9559	*C*-sulfation	C12	Pentosylation, dehydration			+
M26	9.56	413.1633	−0.02	$C_{20}H_{29}O_7S$	331.1908, 287.2008, 79.9559	*C*-sulfation	C12	14-Deoxylation	+	+	+
M27	9.92	429.1584	0.25	$C_{20}H_{29}O_8S$	365.1945, 347.1873, 96.9588, 80.9638	*O*-sulfation	C19	N.A.			+
M28	10.25	413.1634	0.12	$C_{20}H_{29}O_7S$	331.1892, 80.9638	*C*-sulfation	C14	14-Deoxylation		+	+
M29[d]	10.3	545.2063	1.18	$C_{25}H_{37}O_{11}S$	463.2348, 331.1907, 80.9637	*C*-sulfation	C14	Pentosylation, dehydration			+
M30[d]	10.46	431.1743	0.83	$C_{20}H_{31}O_8S$	349.2005, 96.9586, 80.9636	*O*-sulfation	C19	Reduction			+
M31[d]	10.76	411.1480	0.64	$C_{20}H_{27}O_7S$	285.1853, 79.9559	*C*-sulfation	C12	Dehydration			+

Table 2 (*Contd.*)

Peak	t_R (min)	Experimental *m/z*	Error (ppm)	Formula $[M-H]^-$	MS/MS fragments	Sulfation type	Sulfation site	Other biotransformation	U	P	F
M32	11.12	413.1635	0.27	$C_{20}H_{29}O_7S$	331.1913, 283.1702, 80.9638	*C*-sulfation	C14	14-Deoxylation			+
M33[d]	11.19	411.1480	0.78	$C_{20}H_{27}O_7S$	329.1748, 80.9637	*C*-sulfation	C14	Dehydration			+
M34[d]	12.15	411.1478	0.34	$C_{20}H_{27}O_7S$	329.1748, 80.9637	*C*-sulfation	C14	Dehydration			+
M35[a]	12.70	395.2067	0.68	$C_{21}H_{31}O_7$	349.2035, 331.1907, 287.2007	N.A.	N.A.	N.A.	+	+	+
M36	13.49	395.2073	0.92	$C_{21}H_{31}O_7$	349.2035, 331.1911	N.A.	N.A.	Isoandrographolide	+	+	+
M37	14.18	525.2697	0.55	$C_{27}H_{41}O_{10}$	349.2366	N.A.	N.A.	Glucuronidation	+	+	
M38	15.90	507.2231	1.26	$C_{26}H_{35}O_{10}$	331.1907, 175.0238	N.A.	N.A.	Dehydration, glucuronidation		+	
M39	16.73	331.1911	2.25	$C_{20}H_{27}O_4$	287.2018, 255.1731	N.A.	N.A.	14-Deoxylation			+

[a] Parent drug. [b] Commercial obtained. [c] Partial validated. [d] Newly reported metabolites; _: diagnostic fragments; +: detectable; U: urine; P: plasma; F: Feces; N.A.: not applicable.

a DPI at *m/z* 79.96, whereas M28 and M32 yielded a DPI at *m/z* 80.96. Applying the established MS-based fragmentation workflow for sulfation site discrimination, all four metabolites were identified as *C*-sulfated conjugates. Specifically, M13 and M26 were assigned to C12-sulfated conjugates, and M28 and M32 was C14-sulfated conjugates. This structural interpretation was further validated by the observed NLF of 82 Da (*m/z* 413.16 → 331.19), a hallmark fragmentation of *C*-sulfated andrographolide derivatives. The deduced aglycone moiety of these conjugates was 334 Da, corresponding to a 16 Da mass reduction relative to the parent andrographolide, which indicated a deoxygenation modification on the parent scaffold. These assignments were consistent with four previously structurally elucidated metabolites isolated from rat intestinal contents, while deoxygenation occurred at the C14 position.[21] This consistency thus corroborated the accuracy and practical applicability of the established MS-based workflow for the unambiguous discrimination of sulfation sites on the andrographolide scaffold.

Metabolite M19 was eluted at 8.23 min and exhibited a deprotonated molecular ion at *m/z* 427.1431 ($C_{20}H_{27}O_8S$, error 1.09 ppm). Its MS/MS spectra displayed a dominant DPI at *m/z* 79.96, indicative of a *C*-sulfated conjugate, with the sulfation site likely situated at C12. This assignment was corroborated by a NLF of 82 Da, corresponding to the mass transition *m/z* 427.14 → 345.14. The aglycone moiety was deduced to be 348 Da, representing a 2 Da mass reduction relative to the parent andrographolide. Collectively, these mass spectral features enabled the identification of M19 as a dehydrogenated and C12-sulfated metabolite of andrographolide. To the best of our knowledge, M19 represented a previously unreported novel metabolite, which underscored the efficacy and practical applicability of the established MS-based analytical workflow in the discovery of novel sulfated andrographolide derivatives.

Five sulfated metabolites—M4 (retention time 6.72 min), M8 (7.03 min), M17 (8.01 min), M20 (8.34 min), and M30 (10.46 min)—exhibited identical deprotonated molecular ions at *m/z* 431.17, corresponding to the molecular formula $C_{20}H_{31}O_8S$ (error < 1 ppm). In their MS/MS spectra, all metabolites except M30 produced DPI at *m/z* 80.96, suggesting *C*-sulfation at the C14 position. This structural assignment was further corroborated by a consistent NLF of 82 Da (*m/z* 431.17 → 349.20). The aglycone moieties of M4, M8, M17, and M20 were deduced to be 352 Da–2 Da greater than that of the parent compound—indicating the occurrence of reduction.[16] Based on the established fragmentation workflow, an additional 17 *C*-sulfated metabolites were successfully identified, further expanding the repertoire of structurally characterized sulfated metabolites of andrographolide in rats.

3.4.2 Characterization of *O*-sulfated conjugates. Four bis-sulfated metabolites—M1 (retention time: 4.09 min), M5 (6.74 min), M12 (7.40 min), and M21 (8.52 min)—shared a deprotonated molecular ion at *m/z* 493.12, corresponding to the molecular formula $C_{20}H_{29}O_{10}S_2$, and confirming the presence of two sulfate moieties (a bis-sulfation modification) on the andrographolide scaffold. For M1, its MS/MS spectrum displayed a DPI at *m/z* 79.96, indicative of *C*-sulfation at the C12

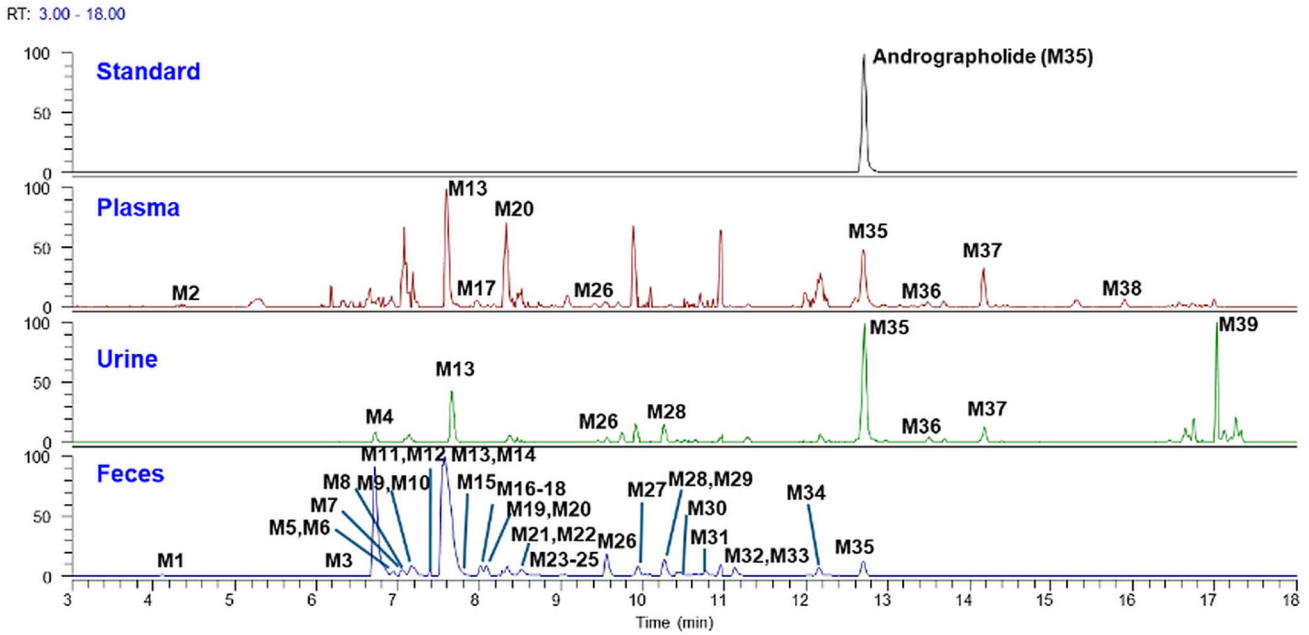

Fig. 6 The extraction ion chromatograms of andrographolide metabolites in rat plasma, urine, and feces.

position. Additionally, a DPI at *m*/*z* 96.96 and a NLF of 80 Da (*m*/*z* 493.12 → 413.16) were observed, consistent with *O*-sulfation at the C3 hydroxyl group. In contrast, M5, M12, and M21 all yielded a DPIs at *m*/*z* 80.96, a signature feature confirming *C*-sulfation at the C14 position. Likewise, the co-occurrence of a DPI at *m*/*z* 96.96 and a NLF of 80 Da (*m*/*z* 493.12 → 413.16) supported an additional *O*-sulfation modification at the C3–OH site. The aglycone moieties of all four metabolites were deduced to be 334 Da, representing 16 Da less than that of the parent compound, suggesting the occurrence of deoxygenation. The sulfation sites inferred from these fragmentation patterns were consistent with those unequivocally confirmed by NMR in a previous report,[21] further validating the accuracy and applicability of the proposed MS-based structural elucidation workflow.

Two metabolites, M9 (retention time: 7.16 min) and M27 (9.92 min), exhibited deprotonated molecular ions at *m*/*z* 429.16, corresponding to the molecular formula $C_{20}H_{29}O_8S$ (error < 1 ppm). Their MS/MS spectra displayed DPIs at *m*/*z* 96.96 and 80.96, indicative of an *O*-sulfate ester located at the aliphatic alcohol group (C19 position). Based on these spectral features, M9 and M27 were identified as C19 *O*-sulfated conjugates of andrographolide.[16] Three additional metabolites—M2 (4.42 min), M16 (7.94 min), and M24 (9.12 min)—shared deprotonated ions at *m*/*z* 449.18 ($C_{20}H_{33}O_9S$, error < 1 ppm). For M16, its MS/MS spectrum showed a DPI at *m*/*z* 96.96 and a NLF of 80 Da (*m*/*z* 449.18 → 369.23), consistent with *O*-sulfation at the C3 hydroxyl group. Likewise, M24 yielded DPIs at *m*/*z* 96.96 and 80.96, confirming *O*-sulfation at the C19 aliphatic alcohol. In contrast, M2 was characterized as a *C*-sulfated conjugate at C14 based on established fragmentation rules. The aglycone moieties of all three metabolites exhibited a molecular weight of 370 Da, which was 20 Da higher than that of the parent drug, implying the occurrence of combined di-reduction and oxidation modifications. In total, twelve metabolites were confirmed to undergo *O*-sulfation, with six sulfated at C3 and the other six at C19.

3.4.3 Characterization of other metabolites. In addition to sulfation, andrographolide underwent additional phase II biotransformation modifications, expanding its *in vivo* metabolic diversity. For instance, M37 exhibited a deprotonated molecular ion at *m*/*z* 525.2697 ($C_{27}H_{41}O_{10}$, error 0.55 ppm) and was eluted at 14.18 min. It was 176 Da higher than that of the parent drug, suggesting glucuronidation. Thus, M37 was tentatively identified as andrographolide glucuronide conjugate. Similarly, M38 showed an $[M–H]^-$ ion at *m*/*z* 525.2697 ($C_{27}H_{41}O_{10}$, error 0.55 ppm) with a retention time of 15.90 min. Its MS/MS spectrum exhibited a neutral loss of 176 Da (*m*/*z* 507.22 → 331.19), confirming the glucuronide conjugation. The aglycone core of M38 was deduced to be 332 Da, indicating an additional dehydration modification. Therefore, M38 was characterized as a dehydrated and glucuronidated metabolite of andrographolide. Sulfated metabolites were also found to undergo subsequent glycosylation. For example, M3, M10, and M15—all identified as C14-sulfated derivatives—displayed a neutral loss of 132 Da (*m*/*z* 463.23 → 331.19), indicative of a pentosyl moiety. The aglycone molecular weight was inferred to be 352 Da, implying the occurrence of a reduction reaction. Accordingly, these metabolites were preliminarily identified as pentosylated, C14-sulfated, and reduced derivatives of andrographolide.

3.5 Proposed metabolic pathways of andrographolide

The proposed metabolic pathways of andrographolide, summarized in Fig. 7 based on the 39 identified metabolites, revealed three principal types of biotransformation. As

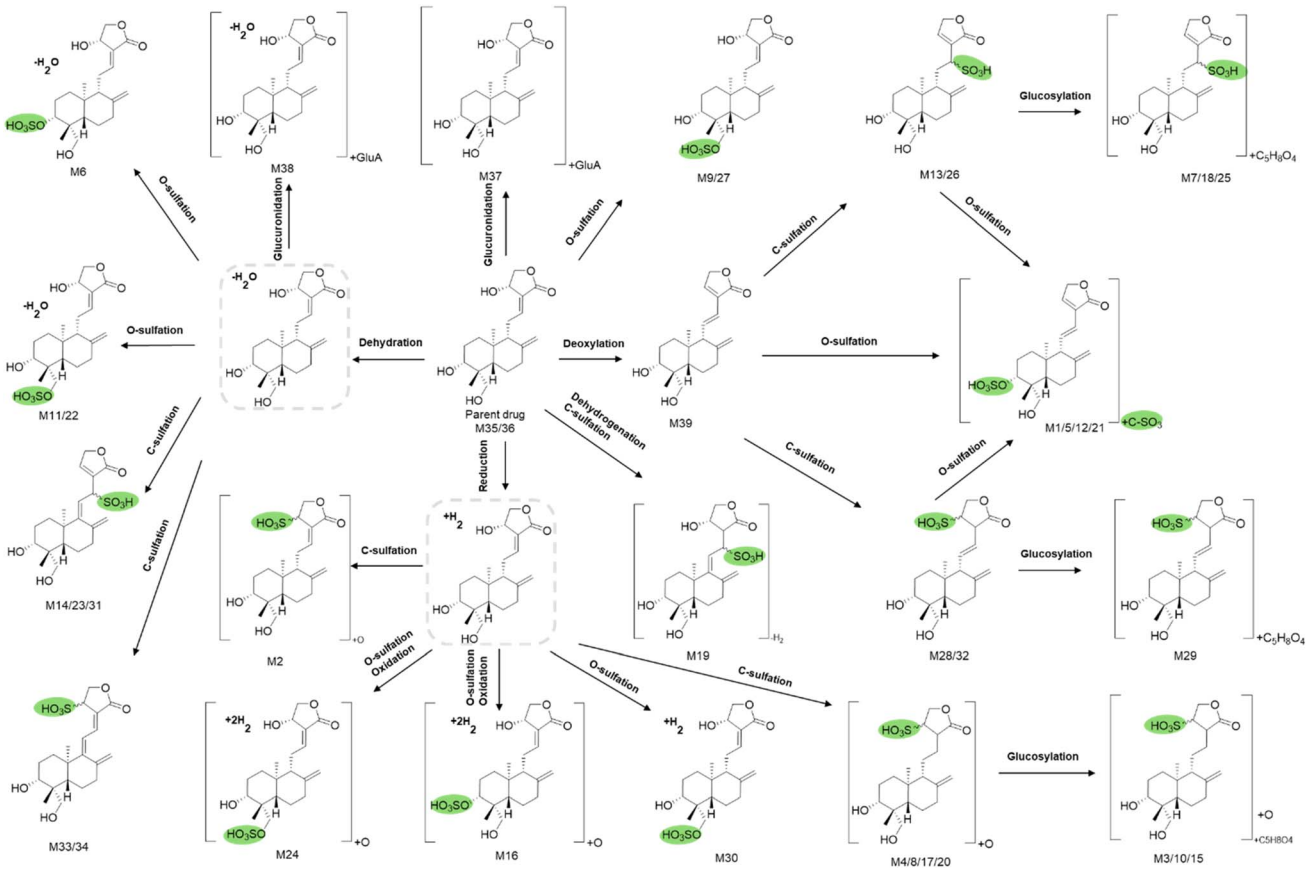

Fig. 7 The proposed metabolic pathways of andrographolide in rat urine, plasma, and feces.

a labdane diterpenoid lactone, andrographolide first underwent primary metabolic reactions including deoxygenation (*e.g.*, M39), reduction, oxidation, dehydrogenation, and dehydration.[16] These metabolites often acted as intermediates for subsequent Phase II conjugation. The second pathway involves sulfation, which occurs in two distinct forms: *C*-sulfation and *O*-sulfation. *C*-sulfation took place predominantly at C12 and C14. Notably, sulfation at C14 (*e.g.*, in M28) was generally preceded by dehydration modification, whereas sulfation at C12 (*e.g.*, M13) proceeded without prior dehydration. In contrast, *O*-sulfation mainly targeted the hydroxyl groups at C3 (*e.g.*, M6) and C19 (*e.g.*, M11). The third metabolic route was glycosylation, which included both unconjugated glucuronides (*e.g.*, M37, M38) and dual-conjugated metabolites bearing both sulfate and glycosyl groups (*e.g.*, M3, M7).

Collectively, both *C*- and *O*-sulfation represented the most structurally diverse metabolic routes for andrographolide in rats. A panel of sulfated conjugates, including M13, M26, M28, and M32, were previously unequivocally identified as *C*-sulfated derivatives of andrographolide *via* nuclear magnetic resonance spectroscopy.[20] Notably, a subset of these sulfated conjugates was generated *via* an HSO_3^--dependent chemical sulfation process rather than sulfotransferases, which implicated a potential contributory role of the gut microbiota in their biogenesis.[29,30] However, due to the absence of a bile duct-cannulated animal model in the current investigation, it was not possible to definitively distinguish between the systemic circulation-derived and intestinal microbiota-mediated biogenesis of sulfated conjugates *in vivo*. This represented a key experimental limitation to fully elucidating the tissue- and microbe-specific origins of andrographolide sulfation in rats.

Although *in vivo* metabolic profiles of andrographolide in humans have been previously reported in the literature,[16,20,21,24,31,32] these characterized profiles are predominantly restricted to urinary matrices, with limited data available for other biological matrices. In contrast, the metabolites characterized in rats in the present study, with sulfated conjugates as the predominant class, were primarily detected in fecal matrices. These findings highlight the presence of striking matrix-dependent interspecies metabolic disparities between humans and rats. Accordingly, a rigorous, quantitative interspecies metabolic comparison of andrographolide necessitates the acquisition of complementary human metabolic profiling data, most critically comprehensive fecal metabolic profiles that mirror the matrix analyzed in the current rat study.

4. Conclusion

The present study provides a comprehensive and systematic characterization of the *in vivo* pharmacokinetic profile and metabolic fate of andrographolide in rats. Pharmacokinetic analysis revealed that andrographolide underwent rapid

systemic elimination and exhibited moderate oral bioavailability. Notably, andrographolide underwent extensive biotransformation *in vivo*, with a total of 39 analytes identified. Among these, 34 sulfated conjugates were detected, establishing sulfation as the most structurally diverse metabolic pathway of andrographolide in rats. By leveraging the established DPI/NLF-guided LC-MS/MS fragmentation workflow, we successfully and unambiguously elucidated four specific sulfation modification sites: *O*-sulfation at the C3 and C19 hydroxyl groups, and *C*-sulfation at the C12 and C14 positions of the andrographolide scaffold. Consistent with previous reports, all sulfated conjugates were detectable in fecal samples, indicating that their biogenesis may be mediated by gut microbiota—an inference that requires further experimental validation. These findings offer valuable insights into the disposition mechanisms of andrographolide and underscore the importance of addressing metabolic stability and its future development as a therapeutic agent.

Author contributions

Xuelin Sun: conceptualization, methodology, formal analysis, data curation, writing-original draft. Yatong Zhang: validation, investigation. Zhanpeng Shang: resources, methodology. Lin Dou: methodology. Tianying Wang: methodology. Jiantao Qiu and Shuang Chen: methodology, supervision, writing – review & editing. All authors read and contributed to the manuscript.

Conflicts of interest

The authors declare no competing financial interests.

Data availability

All data are included in the manuscript and supplementary information (SI) file. Supplementary information: Tables S1 and S2 summarize the validation results for the LC–MS/MS method. Fig. S1 shows the MS/MS fragmentation pattern of the M9 analog. See DOI: https://doi.org/10.1039/d5ra08654j.

Acknowledgements

This work was supported by the National High Level Hospital Clinical Research Funding (No. BJ-2023-200), Shandong Provincial Natural Science Foundation (No. ZR2023MH144) and Shandong Provincial Medical and Health Program (No. 202302050293).

References

1 G. Wang, T. Wen, F. Liu, *et al.*, Two new diterpenoid lactones isolated from Andrographis paniculata, *Chin. J. Nat. Med.*, 2017, **15**, 458–462.
2 S. Phurithap, A. Jaree and P. Tangpromphan, Purification of andrographolide, a bioactive compound for relieving COVID-19 symptoms, from Andrographis paniculata: Extraction and separation using preparative pulse-injection and adsorption–desorption chromatography, *Sep. Purif. Technol.*, 2025, **376**, 133928.
3 V. Sharma, G. Kumar, P. Kumar, *et al.*, Innovative anticancer molecule andrographolide: a concise review of its pharmacological targets, *Nat. Prod. Res.*, 2025, DOI: 10.1080/14786419.2025.245078.
4 M. Z. Y. Choo and C. L. L. Chai, Chapter Two – The polypharmacology of natural products in drug discovery and development, *Annual Reports in Medicinal Chemistry*, Academic Press, New York, 2023, pp. 55–100.
5 Z. Malik, R. Parveen, B. Parveen, *et al.*, Anticancer potential of andrographolide from *Andrographis paniculata* (Burm.f.) Nees and its mechanisms of action, *J. Ethnopharmacol.*, 2021, **272**, 113936.
6 X. Li, W. Yuan, J. Wu, *et al.*, Andrographolide, a natural anti-inflammatory agent: An Update, *Front. Pharmacol*, 2022, **13**, 920435.
7 H. Ilmi, I. R. Pamungkas, L. Tumewu, *et al.*, Analgesic and Antipyretic Activities of Ethyl Acetate Fraction Tablet of *Andrographis paniculata* in Animal Models, *Evid. Based Complement. Alternat. Med.*, 2021, **2021**, 8848797.
8 W. Li, N. Xia, X. Chen, *et al.*, Activity of antibacterial, antiviral, anti-inflammatory in compounds andrographolide salt, *Eur. J. Pharmacol.*, 2014, **740**, 421–427.
9 P. Yarnvitayalert and T. Saleewong, Mathematical Modeling of Andrographolide Therapy Effects and Immune Response in In Vivo Dynamics of SARS-CoV-2 Infection, *Viruses*, 2025, **17**, 891.
10 W. Guo, Y. Sun, W. Liu, *et al.*, Small molecule-driven mitophagy-mediated NLRP3 inflammasome inhibition is responsible for the prevention of colitis-associated cancer, *Autophagy*, 2014, **10**, 972–985.
11 M. Li, X. Yang, C. Guan, *et al.*, Andrographolide sulfonate reduces mortality in Enterovirus 71 infected mice by modulating immunity, *Viral Immunol.*, 2018, **55**, 142–150.
12 S. Peng, N. Hang, W. Liu, *et al.*, Andrographolide sulfonate ameliorates lipopolysaccharide-induced acute lung injury in mice by down-regulating MAPK and NF-κB pathways, *Acta Pharm. Sin. B*, 2016, **6**, 205–211.
13 Z. Shang, Y. Tian, M. Xiong, Y. Yi, X. Qiao and Y. Yang, Characterization of prenylated phenolics in *Glycyrrhiza uralensis* by offline two-dimensional liquid chromatography/mass spectrometry coupled with mass defect filter, *J. Pharm. Biomed. Anal.*, 2022, **220**, 115009.
14 Z. Shang, L. Xu, Y. Xiao, W. Du, R. An, M. Ye and X. Qiao, A global profiling strategy using comprehensive two-dimensional liquid chromatography coupled with dual-mass spectrometry platforms: Chemical analysis of a multi-herb Chinese medicine formula as a case study, *J. Chromatogr. A*, 2021, **1642**, 462021.
15 Z. Shang, L. Xu, Y. Kuang, *et al.*, Simultaneous determination of 35 constituents and elucidation of effective constituents in a multi-herb Chinese medicine formula Xiaoer-Feire-Kechuan, *J. Pharm. Anal.*, 2021, **11**, 717–725.
16 H. Zhao, H. Hu and Y. Wang, Comparative metabolism and stability of andrographolide in liver microsomes from

humans, dogs and rats using ultraperformance liquid chromatography coupled with triplequadrupole and Fourier transform ion cyclotron resonance mass spectrometry, *Rapid Commun. Mass Spectrom.*, 2013, **27**, 1385–1392.

17 T. Yang, C. Xu, Z. T. Wang, *et al.*, Comparative pharmacokinetic studies of andrographolide and its metabolite of 14-deoxy-12-hydroxy-andrographolide in rat by ultra-performance liquid chromatography–mass spectrometry, *Biomed. Chromatogr.*, 2013, **27**, 931–937.

18 F. Xu, S. Fu, S. Gu, *et al.*, Simultaneous determination of andrographolide, dehydroandrographolide and neoandrographolide in dog plasma by LC–MS/MS and its application to a dog pharmacokinetic study of *Andrographis paniculata* tablet, *J. Chromatogr. B*, 2025, **990**, 125–131.

19 Z. Shang, W. Cai, Y. Cao, *et al.*, An Integrated Strategy for Rapid Discovery and Identification of the Sequential Piperine Metabolites in Rats using Ultra High-Performance Liquid Chromatography/High Resolution Mass Spectrometery, *J. Pharm. Biomed. Anal.*, 2017, **146**, 387–401.

20 X. He, J. Li, H. Gao, *et al.*, Four new andrographolide metabolites in rats, *Tetrahedron*, 2003, **59**, 6603–6607.

21 X. He, J. Li, H. Gao, *et al.*, Six New Andrographolide Metabolites in Rats, *Chem. Pharm. Bull.*, 2003, **51**, 586–589.

22 L. Ye, T. Wang, L. Tang, *et al.*, Poor oral bioavailability of a promising anticancer agent andrographolide is due to extensive metabolism and efflux by P-glycoprotein, *J. Pharm. Sci.*, 2011, **100**, 5007–5017.

23 K. M. Giacomini, S. M. Huang and D. Tweedie, Membrane transporters in drug development, *Nat. Rev. Drug Discovery*, 2010, **9**, 215–236.

24 X. He, J. Li, H. Gao, *et al.*, Identification of a rare sulfonic acid metabolite of andrographolide in rats, *Drug Metab. Dispos.*, 2023, **31**, 983–985.

25 C. E. C. A. Hop, Z. Wang, Q. Chen and G. Kwei, Plasma-pooling methods to increase throughput for in vivo pharmacokinetic screening, *J. Pharm. Sci.*, 1998, **87**, 901–903.

26 X. Sun, Z. Shang, Y. Zhang, *et al.*, Comprehensive Investigation of Sweroside Metabolism in Rats Using a De Novo Strategy Based on Ultra-High-Performance Liquid Chromatography/Quadrupole-Exactive Mass Spectrometry, *J. Sep. Sci.*, 2024, **47**, e70048.

27 D. Zheng, J. Shao, W. Chen, *et al.*, In vitro Metabolism of Sodium 9-dehydro-17-hydro-andrographolide-19-yl Sulfate in Rat Liver S9 by Liquid Chromatography–Mass Spectrometry Method, *Pharmacogn. Mag.*, 2016, **12**, 102–108.

28 L. Yi, J. Dratter, C. Wang, *et al.*, Identification of sulfation sites of metabolites and prediction of the compounds' biological effects, *Anal. Bioanal. Chem.*, 2006, **386**, 666–674.

29 D. Tang, W. Hu, B. Fu, *et al.*, Gut microbiota-mediated C-sulfonate metabolism impairs the bioavailability and anti-cholestatic efficacy of andrographolide, *Gut Microbes*, 2024, **16**, 2387402.

30 Z. Huo, X. Feng, Y. Wang, *et al.*, Sulfite as the substrate of C-sulfonate metabolism of α, β-unsaturated carbonyl containing andrographolide: analysis of sulfite in rats' intestinal tract and the reaction kinetics of andrographolide with sulfite, *Chin. J. Nat. Med.*, 2021, **19**, 706–712.

31 L. Cui, F. Qiu and X. Yao, Isolation and identification of seven glucuronide conjugates of andrographolide in human urine, *Drug Metab. Dispos.*, 2005, **33**, 555–562.

32 L. Cui, W. Chan, F. Qiu, *et al.*, Identification of Four Urea Adducts of Andrographolide in Humans, *Drug Metab. Lett.*, 2008, **2**, 261–268.